Plasma membrane translocation of a protein needle based on a triple-stranded β-helix motif.

AUTHOR(S):

Sanghamitra, Nusrat J M; Inaba, Hiroshi; Arisaka, Fumio; Ohtan Wang, Dan; Kanamaru, Shuji; Kitagawa, Susumu; Ueno, Takafumi

CITATION:

Sanghamitra, Nusrat J M ...[et al]. Plasma membrane translocation of a protein needle based on a triple-stranded β-helix motif.. Molecular BioSystems 2014, 10(10): 2677-2683

ISSUE DATE:

2014-08-01

URL:

http://hdl.handle.net/2433/200240

Molecular BioSystems

Cite this: DOI: 10.1039/c0xx00000x

www.rsc.org/xxxxxx

PAPER

Plasma membrane translocation of a protein needle based on a triple-stranded β-helix motif

Nusrat J. M. Sanghamitra,[a] Hiroshi Inaba,[b] Fumio Arisaka,[c] Dan Ohtan Wang,[a] Shuji Kanamaru,[c] Susumu Kitagawa*[a,b] and Takafumi Ueno*[a,c]

Received (in XXX, XXX) Xth XXXXXXXXX 20XX, Accepted Xth XXXXXXXXX 20XX
DOI: 10.1039/b000000x

Plasma membrane translocation is challenging due to the barrier of cell membrane. Contrary to the synthetic cell-penetrating materials, tailed bacteriophages use cell-puncturing protein needles to puncture the cell membranes as an initial step of DNA injection process. Cell-puncturing protein needles are thought to remain functional in the native phages. In this paper, we found that a bacteriophage T4 derived protein needle of 16 nm length spontaneously translocates through the living cell membrane. β-helical protein needle (β-PN) internalizes into human red blood cells that lack endocytic machinery. By comparing the cellular uptake of β-PNs with modified surface charge, it is shown that the uptake efficiency is maximum when it has an negative charge corresponding to a zeta potential value of -16 mV. In HeLa cells, uptake of β-PN incorporates endocytosis independent mechanisms with partial macropinocytosis dependence. The endocytosis dependence of the uptake increases when the surface charges of β-PNs are modified to positive or negative. Thus, these results suggest that natural DNA injecting machinery can serve as an inspiration to design new class of cell-penetrating materials with tailored mechanism.

Introduction

Plasma membrane translocation of exogenous agents is a challenging task because of the semipermeable nature of the plasma membrane of the living cell.[1] Most often natural and engineered cell-penetrating proteins and peptides are designed based on the theory of maximization of net positive charge in which exogenous "protein transduction domains" are appended by integration of the cationic functional groups as positive grafts to enhance the membrane permeability.[2-4] However, in the nature's design of highly efficient DNA injecting needles of viruses such as tailed bacteriophages, a structure based approach is chosen to achieve infection of host cells.[5] Tailed bacteriophages use cell-puncturing needles such as gene product 5 (gp5) of the bacteriophage T4 to puncture the cell membrane, facilitating the translocation of phage DNA into the cytoplasm (Fig. 1a).[5-10] The torque force exerted onto gp5 is thought to be an important factor for penetration and is generated by a conformational change in the bacteriophage T4.[11,12] The key structural feature of the gp5 is its needle structure that is formed by a triple-stranded β-helix (Fig. 1a).[10] The β-helix consists of three monomers that form parallel β-sheets, resulting in a triangular prismatic needle structure.[10] Highly repetitive amino acid sequences in the β-helix create a regular arrangement of amino acid residues on the surface. Since tailed bacteriophages share a common β-helix motif with similar diameters (1.5-2.5 nm) and lengths (4-8 nm), it is possible that the β-helix motif is

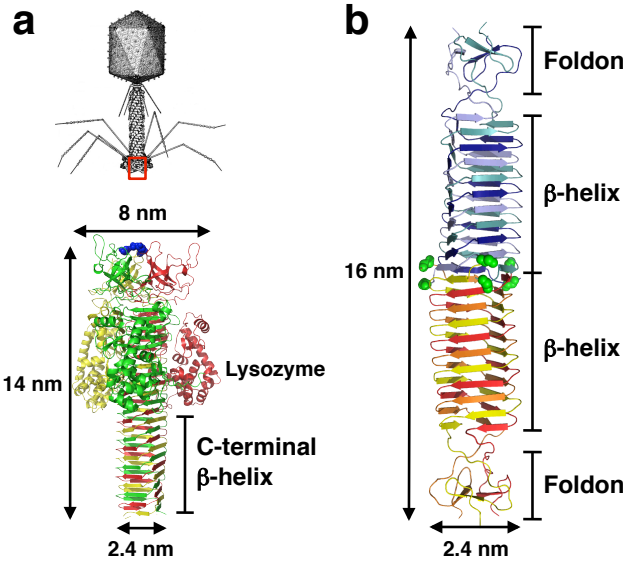

Fig. 1. Structure of β-PN. (a) Crystal structure of gp5 of bacteriophage T4 presented as differently colored monomers.[10] N7 residues are depicted as blue space-filling models. (b) Structure of β-PN presented as differently colored monomers.[13] G18 residues are depicted as green space-filling models.

an essential component of a cell-puncturing needle.[10,14,15] A molecular dynamics simulation suggested that the greater stiffness of the β-helix in comparison to the cell membrane is optimized to maintain the needle structure during penetration.[16,17] Although negative charge of the surface of the β-helix is also anticipated to be important for the membrane-puncturing event, the detailed contribution of the surface charge on the membrane translocation is unknown.[10,18]

The presence of conserved β-helix motif in nature's cell-puncturing needles underscores the possibility of a structural basis of the membrane translocation phenomena. Although few recent studies have highlighted the implication of the protein secondary structure and conformation on cellular internalization of proteins, no clear connection between cellular uptake and their structural propensity is reported.[19-22] A molecular dynamics simulation of membrane penetration of gp5 has indicated the importance of positively and negatively charged residues on the surface of the β-helix of gp5.[12] The charged residues make strong hydrophilic interaction (e.g. H-bonds, charge) with lipids, waters, and neighboring residues, inducing the sliding of the lipids on the β-helix surface. Thus, it is expected that the natural pattern of the charged residues on the β-helix is crucial for the membrane translocation.

Here, we utilized a β-helical protein needle (β-PN) reconstructed from gp5 of the bacteriophage T4 (Fig. 1b)[13] to investigate the membrane translocation of an isolated β-helix motif. β-PNs with different surface charges were synthesized, and the effect of charge on membrane translocation was examined. We demonstrate that β-PN spontaneously internalizes into human red blood cells (hRBCs) that lack endogenous endocytic machinery. The efficiency of uptake was found to depend on the surface charge of the β-PN. Whereas in HeLa cells, we observed that the predominant mechanism of cellular uptake of β-PN was guided by its surface charge. Our results suggest that the inherent structural features of the triple-stranded β-helix motif in β-PN enable it to spontaneously translocate through the membrane. This study demonstrates that natural biosupramolecular machinery may serve as source of inspiration for new approaches to the design of cell-penetrating materials.

Results and discussion

Modification of charged residues on β-PN

The needle structure of β-PN is comprised of a homodimer with twisted triangular prismatic structure formed by intermolecular twist-lock interaction at the N-terminal yielding a β-helical needle of length 16 nm and diameter 2.4 nm (Fig. 1b).[13] The fusion of β-helix motif with foldon at its termini stabilizes the trimer-dimer structure and prevents multimeric aggregation.[13,23] β-PN has alternatively arranged positive (Lys) and negative (Asp, Glu) residues along the rim of the triangular prism (Fig. 2a). Since surface charge plays an important role in most of the cell-penetrating proteins and peptides, in order to illustrate the correlation between the membrane translocation of β-PN and surface charge, we have altered the surface charge of β-PN by chemical modification of surface exposed −COOH (Asp, Glu, and the C-terminus) and $-NH_2$ groups (Lys and the N-terminus) (Fig. 2b). To monitor β-PN in living cells, cysteine residues

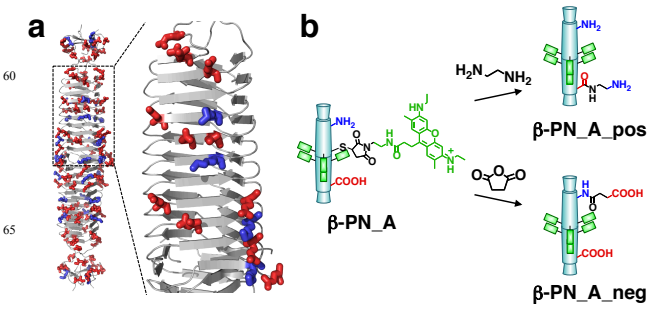

Fig. 2. Modification of charged residues on β-PN. (a) Charged residues on β-PN. Asp and Glu (red) and Lys (blue) are represented as sticks. One of the six sides is enlarged in a detailed view. (b) A schematic drawing of the modification of charged residues of ATTO520-labeled β-PN (β-PN_A). Ethylenediamine was coupled to the –COOH groups of β-PN_A (to generate β-PN_A_pos). Succinic anhydrides were coupled to the $-NH_2$ groups of β-PN_A (to generate β-PN_A_neg).

Table 1. Size and surface charges of the needles

	Hydrodynamic diameter (nm)	Zeta potential (mV)
β-PN_A	10 ± 1.2	–16 ± 1.7
β-PN_A_pos	9.5 ± 1.7	+8.2 ± 0.4
β-PN_A_neg	8.4 ± 1.4	–34 ± 2.7
gp5_A	17 ± 4.8	–24 ± 1.2

The hydrodynamic diameter was measured by DLS using 3 μM protein needle in 0.1 M sodium phosphate, pH 7.0. The surface charge was assessed by zeta potential measurements using 3 μM protein needle in 10 mM sodium phosphate, pH 7.4.

introduced at G18 using site-directed mutagenesis were conjugated with the green fluorescent dye ATTO520-maleimide (Fig. 1b and 2b). MALDI-TOF analysis of β-PN_G18C conjugated with ATTO520 (β-PN_A) indicated a mass increase of 488 Da, which was assigned to an ATTO520-maleimide moiety (calcd. 492 Da), with the complete loss of the peak of the original β-PN_G18C monomer (14,847 Da) (Fig. S1a and S1b). This result indicates that all six G18C residues in β-PN were conjugated to ATTO520-maleimide molecules. The conversion of –COOH groups in β-PN_A to $-NH_2$ groups was achieved by reaction of β-PN_A with ethylenediamine in the presence of *N*-[3-(dimethylamino)propyl]-*N*'-ethylcarbodiimide (EDC) to generate positively charged β-PN_A (β-PN_A_pos) (Fig. 2b). MALDI-TOF analysis of the β-PN_A_pos monomer indicated a molecular weight of 15,975 Da (calcd. 15,962 Da), which accounts for the conjugation of 15 ethylenediamine molecules to each monomer (Fig. S1c). The fifteen surface exposed −COOH groups from Asp and Glu residues and the C-terminus (four –COOH groups, from E78, D99, E104, and E109, of the β-PN_A monomer are buried, Fig. S2) were completely modified. The conversion of $-NH_2$ groups in β-PN_A to –COOH groups was achieved by reaction of β-PN_A with succinic anhydride to generate negatively charged β-PN_A (β-PN_A_neg) (Fig. 2b).

MALDI-TOF analysis of the β-PN_A_neg monomer indicated a molecular weight of 15,850 Da (calcd. 15,836 Da), which accounts for the conjugation of five –COOH groups to each monomer (Fig. S1d). The five surface-exposed $-NH_2$ groups of the six $-NH_2$ groups of Lys residues [$-NH_2$ from K120 is buried (Fig. S2)] and the N-terminus of the β-PN_A monomer were completely modified. Gp5, consisting of the β-helix and three lysozyme domains, was utilized for comparison (Fig. 1a). N7C of gp5_N7C/S351L was modified with ATTO520-maleimide (gp5_A), and complete conjugation was verified by MALDI-TOF analysis (Fig. S1e and S1f). MALDI-TOF mass spectra of each needle include signals assignable to trimer-dimer of β-PN_As and trimer of gp5_A, indicating maintenance of the needle structure after the modifications (Fig. S1). The size of the needles was determined using dynamic light scattering (DLS) (Table 1 and Fig. S3). The modifications did not alter the size of the needles. These results indicate that there is no random aggregation or denaturation of the needle. The surface charge of the needles was determined by zeta potential measurements (Table 1). The zeta potential of β-PN_A (−16 mV) exhibited a negative surface charge in 10 mM sodium phosphate, pH 7.4. In contrast, the zeta potential of β-PN_A_pos (+8.2 mV) exhibited a positive surface charge, whereas the zeta potential of β-PN_A_neg (−34 mV) exhibited a negative surface charge. These results indicate that the surface charge of β-PN_A was successfully altered.

Cellular uptake into hRBCs

hRBCs were used to evaluate the non-endocytic membrane translocation because hRBCs lack endogenous endocytic machinery.[24,25] hRBCs were incubated with the protein needles in an aqueous isotonic solution containing 0.9% (w/v) NaCl for 1 h at 37°C under 5% CO_2. The cells were washed three times and observed using confocal microscopy (Fig. 3a-3d). Internalization of β-PN_A into hRBCs was indicated by the presence of a homogenous green fluorescence due to β-PN_A in the cytoplasm of hRBCs (Fig. 3a). However, endocytic markers such as transferrin and LacCer could not be internalized into hRBCs (Fig. S4).[26] This result suggests that β-PN_A directly translocated through the plasma membrane of hRBCs. In contrast, β-PN_A_pos predominantly accumulated on the membrane (Fig. 3b). This accumulation may be induced by the electrostatic interaction between positively charged β-PN_A_pos (+8.2 mV) and the negatively charged hRBC membrane (–14 mV),[27] thereby prohibiting translocation through the membrane. The uptake efficiency of β-PN_A_pos and β-PN_A_neg was 0.5 and 0.8 times that of β-PN_A, respectively, as shown in Fig. 3e, which shows the uptake efficiency with respect to the zeta potential of each needle. The low translocation efficiency of β-PN_A_neg is expected to result from the greater negative charge (–34 mV) on the β-PN_A_neg surface in comparison to β-PN_A (–16 mV), which induces electrostatic repulsion with the membrane. These results indicate that among all of the protein needles, β-PN_A possesses the ideal surface charge required for membrane translocation. The uptake efficiency of gp5_A was 0.5 times that of β-PN_A (Fig. 3e). The presence of the three lysozyme domains of gp5_A appears to decrease the uptake efficiency (Fig. 1a).

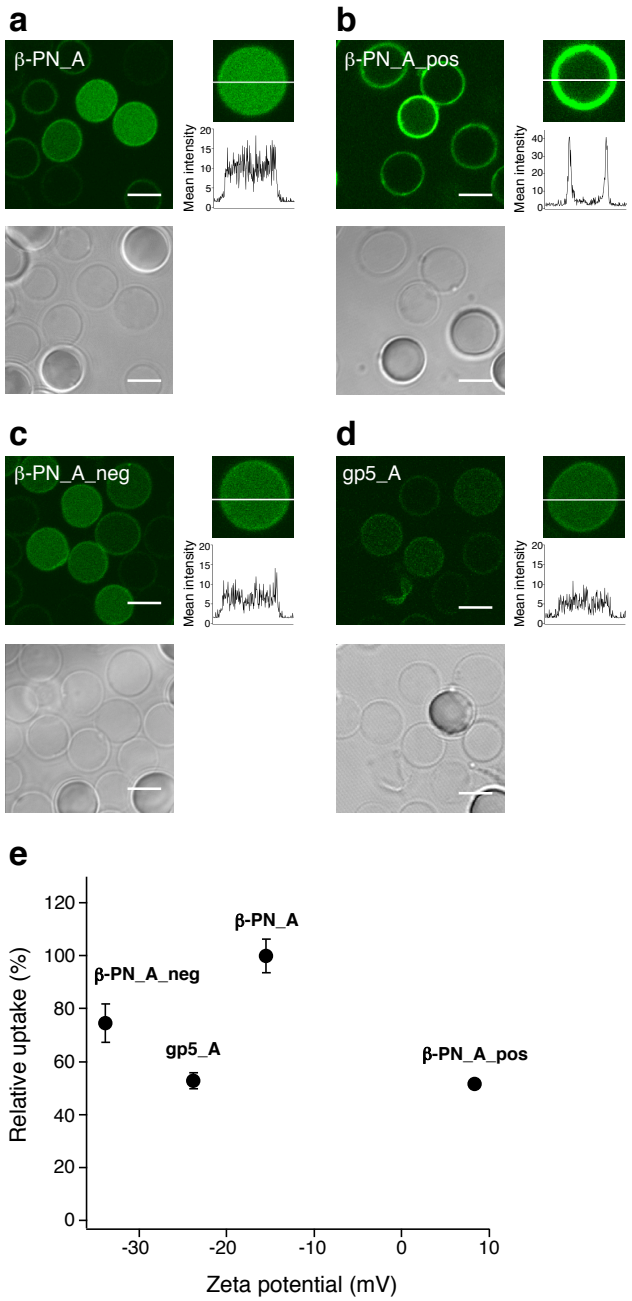

Fig. 3. Non-endocytic uptake into human red blood cells (hRBCs). Confocal fluorescence (top) and bright field (bottom) images of (a) β-PN_A, (b) β-PN_A_pos, (c) β-PN_A_neg, and (d) gp5_A in hRBCs (scale bars, 5 μm). Each needle was incubated with hRBCs for 1 h in 0.9% NaCl at 37°C under 5% CO_2. (e) The uptake efficiency into hRBCs with respect to the zeta potentials of each needle. The relative uptake percentage was determined from the integrated fluorescence intensity of the intracellular section normalized to the area of the section from the respective images (Fig. S5). The data represent mean ± SEM (n = 11). The concentration of ATTO520 was adjusted to 10 μM for comparison of the fluorescence intensity. The concentration of β-PN_A, β-PN_A_pos, and β-PN_A_neg was 1.7 μM, whereas that of gp5_A was 3.3 μM.

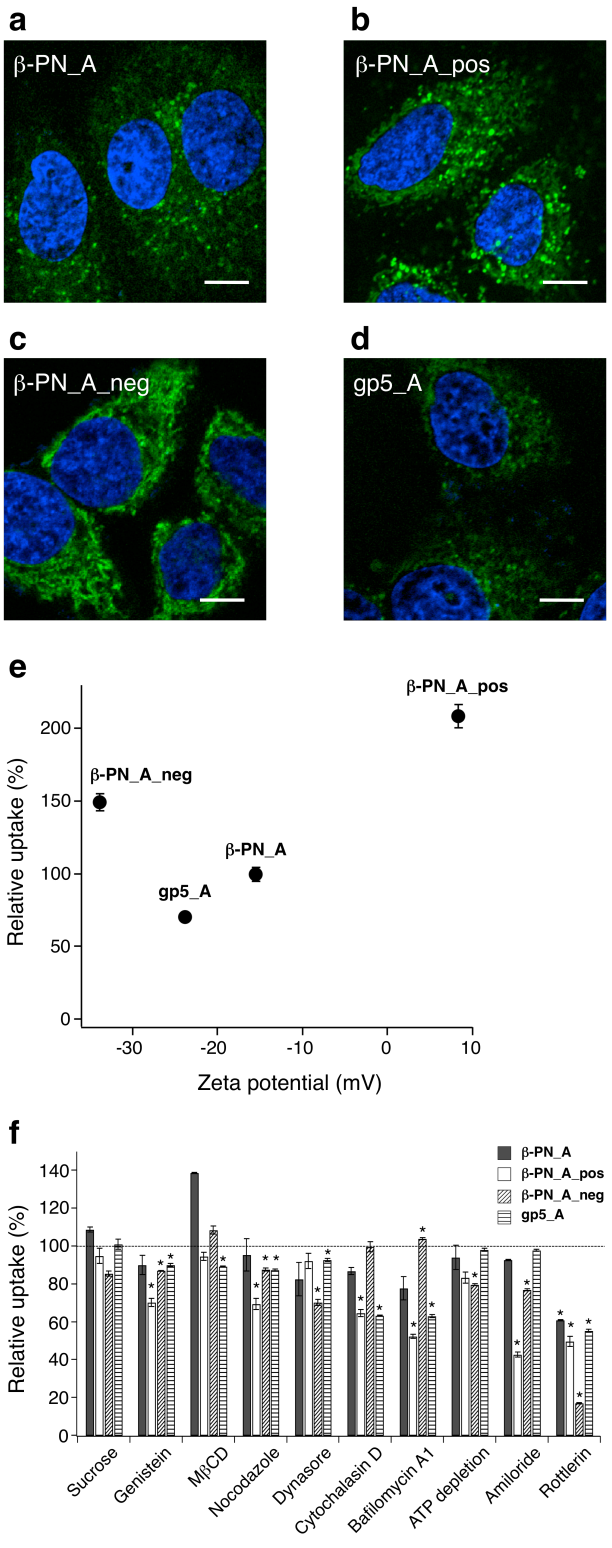

Fig. 4. Uptake into HeLa cells. Confocal fluorescence images of (a) β-PN_A, (b) β-PN_A_pos, (c) β-PN_A_neg, and (d) gp5_A in HeLa cells (scale bars, 10 μm). Each needle was incubated with HeLa cells for 1 h in medium at 37°C under 5% CO_2. Cell nuclei were labeled with blue fluorescent Hoechst 33342. (e) Cellular uptake efficiency into HeLa cells with respect to the zeta potential of each needle. The relative uptake percentage was determined using flow cytometry after incubation for 1 h. The data represent mean ± SEM (n = 3). (f) Flow cytometry analysis indicating the percentage of cells that contained internalized needles following 1 h incubation with HeLa cells that were pretreated with various pharmacological inhibitors of endocytosis, normalized to untreated cells. The relative uptake was normalized using cells which were treated with each needle in the absence of any inhibitor (positive control, 100% uptake). The data represent mean ± SEM (n = 3). *P < 0.05 compared to positive control. The concentration of ATTO520 was adjusted to 5 μM for comparison of the fluorescence intensity. The concentration of β-PN_A, β-PN_A_pos, and β-PN_A_neg was 0.83 μM, whereas that of gp5_A was 1.7 μM.

Cellular uptake into HeLa cells

The uptake mechanism of β-PN_A into typical mammalian cells was evaluated using HeLa cells. Upon incubation of β-PN_A with HeLa cells for 1 h, green fluorescence was observed in the cytoplasm, indicating the internalization of β-PN_A (Fig. 4a). It was confirmed that the needle internalized into HeLa cells without decomposition, aggregation, and cytotoxicity as described in the Supporting Information. In contrast to hRBCs, β-PN_A_pos did not accumulate on the membranes of HeLa cells but was rather internalized (Fig. 4b). β-PN_A_neg and gp5_A were internalized as observed in hRBCs (Fig. 4c and 4d). The uptake efficiency of each needle was compared using flow cytometry analysis after 1 h incubation (Fig. 4e). In contrast to the observations in hRBCs (Fig. 3e), the uptake efficiency of β-PN_A_pos and β-PN_A_neg were 2.1 and 1.5 times that of β-PN_A, respectively. These results suggested that the increase in the uptake efficiency of β-PN_A_pos and β-PN_A_neg in HeLa cells was due to endocytosis. To verify this hypothesis, the internalization efficiency in HeLa cells was evaluated in the presence of different pharmacological inhibitors of endocytosis (Fig. 4f).[26,28] The protein needles were incubated with HeLa cells for 1 h after pretreatment with each inhibitor. Significant inhibition of the cellular uptake of β-PN_A was not observed for any inhibitor (< 22%) except for rottlerin (40%), which has been reported to inhibit macropinocytosis.[29] Because amiloride, which is also an inhibitor of macropinocytosis, exhibited decreased inhibition (7.2%), the uptake of β-PN_A was concluded to be partially dependent on macropinocytosis. Cellular uptake of β-PN_A into HeLa cells was evaluated in the presence of rottlerin using confocal microscopy (Fig. S6). Homogeneous green fluorescence with disappearance of dot-like structures in cytoplasm clearly indicated non-endocytic uptake of β-PN_A. For β-PN_A_pos, significant inhibition of the uptake by several inhibitors in comparison to β-PN_A revealed the dependence on multiple endocytic pathways (Fig. 4f). Uptake of β-PN_A_neg and β-PN_A was primarily inhibited by rottlerin, but the inhibitory efficiency (83%) was greater for β-PN_A_neg than for β-PN_A (Fig. 4f). For gp5_A, cell uptake was inhibited by several inhibitors, including cytochalasin D, bafilomycin A1, and rottlerin, indicating a dependence on multiple endocytic pathways (Fig. 4f). These results indicated that β-PN_A exhibits the least dependence on endocytosis among all of the needles, whereas β-PN_A_pos and β-PN_A_neg were highly dependent on this mechanism.

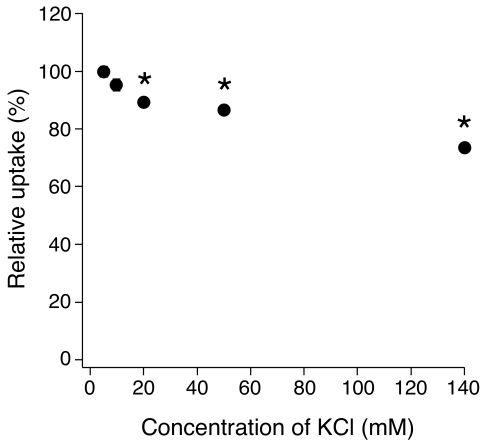

Fig. 5. KCl-dependence on relative uptake percentage of β-PN_A into HeLa cells. β-PN_A (0.83 μM) was incubated with HeLa cells in the medium with various concentrations of KCl for 1 h at 37°C under 5% CO_2. The relative uptake percentage was determined using flow cytometry. The data represent mean ± SEM (n = 3). *P < 0.05 compared to cells that were treated with β-PN_A in the medium containing 5 mM KCl.

Membrane potential dependence of cellular uptake of β-PN_A

While cellular uptake of β-PN_A in hRBCs and HeLa cells could prove the non-endocytic mode of cell entry of β-PN_A, it is important to explain the driving force required for this process. Membrane potential has been reported to provide the energy for the DNA internalization during the infection process of bacteriophages T4, T7, and P22.[8,30-33] Therefore, the uptake efficiency of β-PN_A in HeLa cells was evaluated in the presence of different concentrations of extracellular KCl that reduces the membrane potential of viable cells.[34] The uptake efficiency was decreased with increasing extracellular KCl concentration (Fig. 5). One of the reasons of the decreased uptake efficiency is expected to be due to inhibition of cellular binding of negatively charged β-PN_A by decrease of membrane potential as reported in anionic nanoparticle.[35]

Discussion

Comparison of the cellular uptake of the evaluated protein needles into hRBCs and HeLa cells revealed the effect of the surface charge of the protein needles on the mechanism and the efficiency of membrane translocation. In hRBCs, β-PN_A with a threshold value of -16 mV exhibited a non-endocytic mode of membrane translocation with the highest efficiency among all of the protein needles (Fig. 3e). In contrast, β-PN_A_pos that has a zeta potential value of +8.2 mV predominantly adsorbed on the membrane surface owing to the strong electrostatic interaction with the negatively charged hRBC membrane, as shown in Fig. 3b.[27] Increase in the negative charge as in the case of β-PN_A_neg with a zeta potential value of -34 mV reduces the efficiency of membrane translocation. It is expected to be due to stronger repulsion with the hRBC surface. In the HeLa cells, the uptake efficiency was the highest for β-PN_A_pos (Fig. 4e). The endocytosis inhibition studies indicated that the uptake of β-PN_A_pos was induced by several endocytosis- and macropinocytosis-dependent pathways due to electrostatic interaction with HeLa cell membranes, like that of positively charged cell-penetrating peptides and proteins (Fig. 4f).[3,36-39] Whereas β-PN_A translocates through the membrane predominantly with the non-endocytic mode due to electrostatic repulsion to the membranes though 40% contribution of macropinocytosis is also present, in agreement with study of differently charged polymers.[40] The uptake efficiency of β-PN in HeLa cells was about half of that of positively charged cell-penetrating peptide, octaarginine (R8) (Supporting Information, Fig. S11).[41] The mechanism of membrane translocation of β-PN_A_neg is predominantly the macropinocytosis pathway induced by the stronger negative charge on β-PN_A_neg compared to β-PN_A, as observed for negatively charged polymers (Fig. 4f).[40] These results suggest that the amount of negative charge on β-PN_A is appropriate to facilitate the non-endocytic mode of membrane translocation in both hRBCs and HeLa cells.

The spontaneous membrane translocation of β-PN_A provides insight into the mechanism of infection of tailed bacteriophages. The infection of some tailed bacteriophages has been reported to require a membrane potential.[8,30-33] However, it is not yet clear which step of infection is driven by the membrane potential.[8] The membrane translocation of β-PN_A into HeLa cells is dependent on the extracellular KCl concentration. Since higher extracellular KCl decreases the membrane potential,[34] our result suggests that the membrane potential may be one of the driving forces that govern the β-PN_A membrane translocation process. Therefore, membrane puncturing by protein needles during bacteriophage infection may represent the step that requires a membrane potential.

Conclusions

We found membrane translocation of the protein needles derived from bacteriophage T4 and provided a structural insight into the mechanism. We envision that β-helix motif based protein needles can be utilized for efficient *in vitro* and *in vivo* delivery of large molecular cargos, such as proteins and nucleic acids, directly into the cytoplasm. Therefore, this study presents a new approach of designing cell-penetrating materials from the natural biosupramolecular machineries. Since the terminal structure of β-PN is expected to be important for attachment to the membrane, modification of foldon domain of β-PN is in progress to elucidate the detailed mechanism of the membrane translocation of β-PN.

Experimental section

Labeling with ATTO520

β-PN_A: A DMSO solution of ATTO520-maleimide (ATTO-TEC, 60 μM) was slowly added to an aqueous solution of β-PN_G18C (5 μM in 20 mM potassium phosphate, pH 7.0), and the mixture (final concentration of 5% DMSO) was gently stirred at 25°C for 15 h in the dark. β-PN_A was purified using Sephadex G-25 that was equilibrated with 0.1 M sodium phosphate, pH 7.0. MS (MALDI-TOF): [β-PN_G18C monomer + ATTO520-maleimide]$^+$, calcd.: 15,335; found: 15,331. Gp5_A: A DMSO solution of ATTO520-maleimide (105 μM) was slowly added to an aqueous solution of gp5_N7C/S351L (7 μM in 20

mM Tris-HCl, pH 8.0, 0.2 M NaCl, 0.5 mM TCEP-HCl), and the mixture (final concentration of 5% DMSO) was gently stirred at 18°C for 3 h in the dark. Gp5_A was purified using Sephadex G-25 that was equilibrated with 0.1 M sodium phosphate, pH 7.0. MS (MALDI-TOF): [gp5_N7C/S351L monomer + ATTO520-maleimide]$^+$, calcd.: 64,747; found: 65,275.

Modification of the surface charge of β-PN_A

β-PN_A_pos: β-PN_A (2.0 μM in 0.1 M sodium phosphate, pH 7.0) was slowly added to an aqueous solution of ethylenediamine dihydrochloride (1.6 M in 0.1 M sodium phosphate, pH 7.0). EDC was added to the mixture (final concentration: 10 mg/mL). The mixture was gently stirred at 25°C for 5 h in the dark. β-PN_A_pos was purified using Sephadex G-25 that was equilibrated with 0.1 M sodium phosphate, pH 7.0. MS (MALDI-TOF): [β-PN_G18C monomer + ATTO520-maleimide + 15 $-NH_2$ modifications]$^+$, calcd.: 15,962; found: 15,975. β-PN_A_neg: A DMSO solution of succinic anhydride (18 mM) was slowly added to an aqueous solution of β-PN_A (5.0 μM in 0.1 M sodium carbonate, pH 9.0), and the mixture (final concentration of 10% DMSO) was gently stirred at 25°C for 16 h in the dark. β-PN_A_neg was purified using Sephadex G-25 that was equilibrated with 0.1 M sodium phosphate, pH 7.0. MS (MALDI-TOF): [β-PN_G18C monomer + ATTO520-maleimide + 5 −COOH modifications]$^+$, calcd.: 15,836; found: 15,850.

Confocal imaging of hRBCs

hRBCs (3×10^5 cells) in a 0.9% NaCl solution were plated onto single-well glass-bottom dishes, which were coated with 1.2 mg/mL poly-L-lysine for 3 h and subsequently washed with 0.9% NaCl. The cells were allowed to adhere by incubation for 1 h at 37°C under 5% CO_2. After washing with 0.9% NaCl, β-PN_A, β-PN_A_pos, β-PN_A_neg (each at a concentration of 1.7 μM), or gp5_A (3.3 μM) were added and incubated for 1 h. The concentration of ATTO520 was adjusted to 10 μM for comparison of the fluorescence intensity. The cells were washed with a 0.9% NaCl solution and imaged (excitation using a 488-nm laser and observed through a 525/50 emission filter). Uptake efficiency into the cells was quantified from the integrated fluorescence intensity of the intracellular section that was normalized to the area of the section (Fig. S5). Eleven cells were analyzed for each sample to calculate the intensity to obtain the average value and standard deviation. Dextran Oregon Green® 488; 70,000 MW (Invitrogen), which cannot be internalized into red blood cells, was used as a negative control.[42]

Experiments with HeLa cells

Confocal imaging

HeLa cells (2.0×10^4 cells) were plated onto single-well glass-bottom dishes and cultured in cell culture medium at 37°C under 5% CO_2 for 12 h. β-PN_A, β-PN_A_pos, β-PN_A_neg (each at a concentration of 0.83 μM), or gp5_A (1.7 μM) were added and incubated for 1 h. The concentration of ATTO520 was adjusted to 5 μM for comparison of the fluorescence intensity. The medium was removed, and the cells were washed with 1× HBSS. The nucleus was labeled with Hoechst 33342 (5 μg/mL) (Invitrogen) by incubating the cells with the dye solution in HBSS for 15 min at 37°C under 5% CO_2. The dye solution was removed, and the cells were washed with 1 × HBSS. Imaging was performed in fresh cell culture medium. ATTO520-labeled samples, Hoechst 33342 were excited with 488 nm and 405 nm lasers and were observed through 525/50 and 450/50 emission filters, respectively.

Cellular uptake analysis

HeLa cells (1.3×10^5 cells) were plated in 1.5 cm dishes and cultured in cell culture medium at 37°C under 5% CO_2 for 12 h. β-PN_A, β-PN_A_pos, β-PN_A_neg (each at a concentration of 0.83 μM), or gp5_A (1.7 μM) were added to the cells and incubated for 1 h. The culture medium was removed, and the cells were washed with 1 × PBS. The cells were collected by trypsinization and centrifugation followed by suspension in 1 × PBS with 5% FBS. Cellular uptake was analyzed using flow cytometry. Each sample was analyzed three times.

Inhibition of endocytosis

For all inhibition studies, HeLa cells (2×10^5 cells) were plated in 1.5 cm dishes and cultured in cell culture medium at 37°C under 5% CO_2 for 12 h. The cells were preincubated with endocytic inhibitors (400 μM genistein, 5 μg/mL nocodazole, 50 μM cytochalasin D, or 40 nM bafilomycin A1 for 1 h and 0.45 M sucrose, 3 mM MβCD, 80 μM dynasore, 10 mM NaN_3 with 50 mM 2-deoxy-D-glucose for ATP depletion, 4 mM amiloride, or 10 μM rottlerin for 30 min) in cell culture medium without FBS. The cells were washed and incubated with β-PN_A, β-PN_A_pos, β-PN_A_neg (each at a concentration of 0.83 μM), or gp5_A (1.7 μM) for 1 h. The cells were washed with 1 × PBS, and cellular uptake was analyzed using flow cytometry as previously described. Each sample was analyzed three times. Inhibition conditions were optimized by analyzing the uptake of endocxytosis markers after incubation of 16.7 μg/mL human Transferrin (hTf)-AlexaFluor488 (Invitrogen) or 0.81 μM BSA-complexed BODIPY FL C5-Lactosylceramind (LacCer) (Invitrogen) for 15 min and 0.5 mg/mL Oregon Green labeled 70 kDa dextran (Invitrogen) for 3 h in HeLa cells that were pretreated with the endocytosis inhibitors, as previously described.[26]

Acknowledgement

We thank Professor N. Nakatsuji and Dr. K. Aiba for supplying HeLa cells and permission for flow cytometry measurement, S. Kobayashi for assistance with cell experiments and CeMI for assistance with confocal microscopy. This work was supported by a Research Fellowship for Young Scientists of JSPS for H.I. (No. 4240) and NEXT program for T.U. from JSPS and TOKUYAMA SCIENCE FOUNDATION, Japan. iCeMS is supported by the World Premier International Research Initiative (WPI), MEXT, Japan.

Notes and references

[a] *Institute for Integrated Cell-Material Sciences (WPI-iCeMS), Kyoto University, Yoshida, Sakyo-ku, Kyoto 606-8501, Japan. E-mail: kitagawa@icems.kyoto-u.ac.jp, tueno@bio.titech.ac.jp*
[b] *Department of Synthetic Chemistry and Biological Chemistry, Graduate School of Engineering, Kyoto University, Katsura, Nishikyo-ku, Kyoto 615-8510, Japan.*

[c] *Department of Biomolecular Engineering, Graduate School of Bioscience and Biotechnology, Tokyo Institute of Technology, Nagatsuta-cho, Midori-ku, Yokohama 226-8501, Japan.*

† Electronic Supplementary Information (ESI) available: Experimental methods, MALDI-TOF, DLS, ultracentrifugation, GPC, colocalization and MTT assay data. See DOI: 10.1039/b000000x/

1. W. Wickner, *Science*, 2005, **310**, 1452–1456.
2. S. M. Fuchs and R. T. Raines, *ACS Chem. Biol.*, 2007, **2**, 167–170.
3. B. R. McNaughton, J. J. Cronican, D. B. Thompson, and D. R. Liu, *Proc. Natl. Acad. Sci. U.S.A.*, 2009, **106**, 6111–6116.
4. J. S. Wadia, R. V. Stan, and S. F. Dowdy, *Nat Med*, 2004, **10**, 310–315.
5. E. Goldberg, L. Grinus, and L. Letellier (J. D. Karam, Ed.), *Molecular Biology of Bacteriophage T4*, pp 347–356, American Society for Microbiology, Washington DC, 1994.
6. P. G. Leiman, S. Kanamaru, V. V. Mesyanzhinov, F. Arisaka, and M. G. Rossmann, *Cell. Mol. Life Sci.*, 2003, **60**, 2356–2370.
7. M. G. Rossmann, V. V. Mesyanzhinov, F. Arisaka, and P. G. Leiman, *Curr. Opin. Struct. Biol.*, 2004, **14**, 171–180.
8. I. J. Molineux and D. Panja, *Nat. Rev. Microbiol.*, 2013, **11**, 194–204.
9. P. Cotter, *Nature*, 2011, **475**, 301–303.
10. S. Kanamaru, P. G. Leiman, V. A. Kostyuchenko, P. R. Chipman, V. V. Mesyanzhinov, F. Arisaka, and M. G. Rossmann, *Nature*, 2002, **415**, 553–557.
11. V. A. Kostyuchenko, P. R. Chipman, P. G. Leiman, F. Arisaka, V. V. Mesyanzhinov, and M. G. Rossmann, *Nat. Struct. Mol. Biol.*, 2005, **12**, 810–813.
12. W. Nishima, S. Kanamaru, F. Arisaka, and A. Kitao, *J. Am. Chem. Soc.*, 2011, **133**, 13571–13576.
13. N. Yokoi, H. Inaba, M. Terauchi, A. Z. Stieg, N. J. M. Sanghamitra, T. Koshiyama, K. Yutani, S. Kanamaru, F. Arisaka, T. Hikage, A. Suzuki, T. Yamane, J. K. Gimzewski, Y. Watanabe, S. Kitagawa, and T. Ueno, *Small*, 2010, **6**, 1873–1879.
14. C. Browning, M. M. Shneider, V. D. Bowman, D. Schwarzer, and P. G. Leiman, *Structure*, 2012, **20**, 326–339.
15. K. Harada, E. Yamashita, A. Nakagawa, T. Miyafusa, K. Tsumoto, T. Ueno, Y. Toyama, and S. Takeda, *Biochim. Biophys. Acta*, 2013, **1834**, 284–291.
16. S. Keten, J. F. R. Alvarado, S. Müftü, and M. J. Buehler, *Cell. Mol. Bioeng.*, 2009, **2**, 66–74.
17. S. Keten, Z. Xu, and M. J. Buehler, *Mater. Sci. Eng. C*, 2011, **31**, 775–780.
18. A. V. Kajava and A. C. Steven, *Adv. Protein Chem.*, 2006, **73**, 55–96.
19. I. D. Alves, C. Bechara, A. Walrant, Y. Zaltsman, C.-Y. Jiao, and S. Sagan, *PLoS ONE*, 2011, **6**, e24096.
20. A. D. Bautista, J. S. Appelbaum, C. J. Craig, J. Michel, and A. Schepartz, *J. Am. Chem. Soc.*, 2010, **132**, 2904–2906.
21. M. J. Morris, D. Liu, L. M. Weaver, P. G. Board, and M. G. Casarotto, *PLoS ONE*, 2011, **6**, e17864.
22. J. Ren, K. Kachel, H. Kim, S. E. Malenbaum, and R. John, *Science*, 1999, **284**, 955–957.
23. Y. Z. Tao, S. V. Strelkov, V. V. Mesyanzhinov, and M. G. Rossmann, *Structure*, 1997, **5**, 789–798.
24. M. Geiser, B. Rothen-Rutishauser, N. Kapp, S. Schurch, W. Kreyling, H. Schulz, M. Semmler, V. I. Hof, J. Heyder, and P. Gehr, *Environ. Health Perspect.*, 2005, **113**, 1555–1560.
25. T. Wang, J. Bai, X. Jiang, and G. U. Nienhaus, *ACS Nano*, 2012, **6**, 1251–1259.
26. D. Vercauteren, M. Piest, L. J. van der Aa, M. Al Soraj, A. T. Jones, J. F. J. Engbersen, S. C. De Smedt, and K. Braeckmans, *Biomaterials*, 2011, **32**, 3072–3084.
27. H. P. Fernandes, C. L. Cesar, and M. de L. Barjas-Castro, *Rev. Bras. Hematol. Hemoter.*, 2011, **33**, 297–301.
28. S. Xiang, H. Tong, Q. Shi, J. C. Fernandes, T. Jin, K. Dai, and X. Zhang, *J. Controlled Release*, 2012, **158**, 371–378.
29. K. Sarkar, M. J. Kruhlak, S. L. Erlandsen, and S. Shaw, *Immunology*, 2005, **116**, 513–524.
30. L. Letellier, L. Plancon, M. Bonhivers, and P. Boulanger, *Res. Microbiol.*, 1999, **150**, 499–505.
31. B. Labedan and E. B. Goldberg, *Proc. Natl. Acad. Sci. U.S.A.*, 1979, **76**, 4669–4673.
32. P. Kemp, M. Gupta, and I. J. Molineux, *Mol. Microbiol.*, 2004, **53**, 1251–1265.
33. G. L. Perez, B. Huynh, M. Slater, and S. Maloy, *J. Bacteriol.*, 2009, **191**, 135–140.
34. D. F. Baxter, M. Kirk, A. F. Garcia, A. Raimondi, M. H. Holmqvist, K. Flint, D. Bojanic, P. S. Distefano, R. Curtis, and Y. Xie, *J. Biomol. Screen.*, 2002, **7**, 79–85.
35. E. H. Shin, Y. Li, U. Kumar, H. V. Sureka, X. Zhang, and C. K. Payne, *Nanoscale*, 2013, **5**, 5879–5886.
36. H. Hirose, T. Takeuchi, H. Osakada, S. Pujals, S. Katayama, I. Nakase, S. Kobayashi, T. Haraguchi, and S. Futaki, *Mol. Ther.*, 2012, **20**, 984–993.
37. T. Takeuchi, M. Kosuge, A. Tadokoro, Y. Sugiura, M. Nishi, M. Kawata, N. Sakai, S. Matile, and S. Futaki, *ACS Chem. Biol.*, 2006, **1**, 299–303.
38. A. Joliot and A. Prochiantz, *Nat. Cell Biol.*, 2004, **6**, 189–196.
39. J. P. Richard, K. Melikov, E. Vives, C. Ramos, B. Verbeure, M. J. Gait, L. V. Chernomordik, and B. Lebleu, *J. Biol. Chem.*, 2003, **278**, 585–590.
40. J. Liu, H. Bauer, J. Callahan, P. Kopečková, H. Pan, and J. Kopeček, *J. Controlled Release*, 2010, **143**, 71–79.
41. S. Futaki, T. Suzuki, W. Ohashi, T. Yagami, S. Tanaka, K. Ueda, and Y. Sugiura, *J. Biol. Chem.*, 2001, **276**, 5836–5840.
42. Y.-J. Lee, G. Johnson, and J.-P. Pellois, *Biochemistry*, 2010, **49**, 7854–7866.